COMPDYN 2011
3rd ECCOMAS Thematic Conference on
Computational Methods in Structural Dynamics and Earthquake Engineering
M. Papadrakakis, M. Fragiadakis, V. Plevris (eds.)
Corfu, Greece, 25–28 May 2011

INTERFACE TREATMENT IN COMPUTATIONAL FLUID-STRUCTURE INTERACTION

Thomas Klöppel, Alexander Popp and Wolfgang A. Wall

Institute for Computational Mechanics, Technische Universität München
Boltzmannstr. 15, 85748 Garching b. München, Germany
e-mail: {kloeppel,popp,wall}@lnm.mw.tum.de

Keywords: Fluid-Structure Interaction, Non-Matching Meshes, Mortar Method, Dual Lagrange Multipliers, Finite Elements.

Abstract. *Computational approaches for the simulation of fluid-structure interaction (FSI) problems have received much attention in recent years and their importance is still continuously growing. The main reason for this is that FSI problems are of great relevance in all fields of engineering (civil, mechanical, aerospace, bio, etc.) as well as in the applied sciences. In order to develop robust, reliable and efficient methods a number of challenges have to be met. This contribution focuses on the important question of how to treat the interface between solid and fluid. The topic is addressed by reviewing our novel, recently proposed method for dealing with non-matching grids in the context of moving grid FSI schemes. In contrast to available approaches in the literature, the proposed formulation is based on a mortar method with so-called dual Lagrange multipliers and handles the additional complexity of coupling non-matching interface meshes at negligible computational cost. Owing to its generality, the resulting FSI framework does not introduce any restriction on the particular choice of finite element formulations neither for fluid, ALE nor structure. It allows for the application of state-of-the-art iterative solution methods to the resulting system matrices in a straightforward manner and shows an excellent performance within monolithic FSI coupling algorithms.*

1 INTRODUCTION

The numerical simulation of fluid-structure interaction (FSI) phenomena has long been a field of intensive research owing to its many applications in civil, mechanical, aerospace and biomechanical engineering. Of particular interest is the interaction of incompressible flow with flexible structures undergoing finite deformations. We discuss here the most important features of our recently proposed dual mortar finite element method for dealing with non-matching interface meshes in the context of moving grid FSI schemes and monolithic coupling algorithms. The present contribution is thus a shortened version of our article [1] to which we refer for full technical details, more profound discussion of the methods and further numerical examples.

Possible solution strategies for FSI problems range from weakly coupled partitioned over strongly coupled partitioned to monolithic schemes. It could be shown that for some challenging numerical problems such as collapsible tubes [2], thin-walled structures in the hemodynamic or respiratory system [3] or balloon-like problems of human red blood cells [4], monolithic coupling schemes outperform partitioned approaches or are even the only feasible schemes to solve the problem at all. The issue of efficient and robust solvers for monolithic FSI scheme has among others been addressed in [5] where a novel algebraic multigrid preconditioner has been proposed. In general and also in [5], monolithic schemes are derived based on the assumption of a conforming interface discretization, i.e. fluid and structure share a common interface mesh. But only in very rare cases, this assumption will hold. Due to a manifold of reasons one generally has to deal with non-matching grids at the fluid-structure interface. Most often different resolution requirements in the different physical domains or quite simply the presence of complex interface geometries (e.g. in patient-specific biomechanics modeling) make the creation of matching fluid and structure meshes cumbersome or even impossible.

A possible remedy is provided by the mortar method, which has originally been introduced in the context of non-overlapping domain decomposition [6]. A characteristic feature of the mortar method is the imposition of interface constraints in a variationally consistent manner based on Lagrange multipliers. This approach has seen a great thrust of research over the past decade. New fields of application such as finite deformation contact analysis [7, 8, 9, 10] have been established and the mathematical understanding concerning the choice of adequate discrete Lagrange multiplier spaces has been deepened [11, 12, 13, 14].

Different other coupling methods for non-conforming interfaces in the framework of fluid-structure problems have been discussed for example in [15, 16, 17, 18, 19]. However, those contributions are limited to 2D analysis [16, 18] or only consider partitioned coupling schemes. The mortar method is referred to as a method with desirable mathematical and numerical properties [15, 17], but it has not yet been used for FSI computations in a competitive manner. It is obvious that a straightforward application of the standard mortar method will raise numerical issues in the case of monolithic FSI schemes. The Lagrange multiplier degrees of freedom lead to a global system matrix with increased size and saddle point structure. Especially the latter limits the practical use of this approach, since most iterative solvers rely on a matrix structure with only non-zero diagonal entries. A condensation could remedy this problem but would necessitate the inversion of a large matrix and is hence not feasible for practical purposes.

To overcome the numerical issues of the standard mortar method discussed above, we employ a so-called dual mortar method [11, 12, 13, 14] with discrete Lagrange multipliers that are constructed based on a biorthogonality relation with the primal shape functions at the fluid-structure interface. In contrast to standard mortar methods, the dual mortar approach allows for an elimination of the additional degrees of freedom by condensation at negligible computational

cost in the monolithic setting. This ensures that there are only non-zero diagonal entries in the global system matrix. We show that state-of-the-art iterative solvers for monolithic FSI systems with matching interface meshes as proposed in [5] can be applied to the resulting global system matrices without any conceptual changes.

The remainder of this article is organized as follows: The next section briefly introduces the mechanical problem and states the governing equations as well as the weak forms. In section 3 the resulting monolithic system of equations after discretization and consistent linearization is presented and we give some details on dual mortar coupling as well as on condensation of the Lagrange multiplier degrees of freedom. Section 4 demonstrates the validity of the proposed approach with a representative numerical example, and in section 5 we conclude the findings.

2 PROBLEM DESCRIPTION

FSI problems can formally be described as four field problems. To begin with, there are two physical fields, fluid and structure. Furthermore, to account for deformations of the fluid domain, an arbitrary Lagrangian-Eulerian (ALE) approach is employed, constituting a third, non-physical mesh field later also called ALE field. Fluid and structure share a common FSI interface Γ, but not necessarily a common finite element discretization of Γ. Therefore, coupling conditions are applied in a weak sense, introducing a field of Lagrange multipliers on Γ.

2.1 Fluid

The present FSI approach is not limited to a specific flow description. For the sake of brevity we assume a fluid field governed by the instationary, incompressible Navier-Stokes equations for a Newtonian fluid on a deformable fluid domain Ω^{F}. The unknown fluid domain deformation $\mathbf{d}^{\mathrm{G}}$ is defined by a unique mapping $\boldsymbol{\varphi}$ given by

$$\mathbf{d}^{\mathrm{G}}(\mathbf{x},t) = \boldsymbol{\varphi}\left(\mathbf{d}_{\Gamma}^{\mathrm{G}},\mathbf{x},t\right) \quad \text{in} \quad \Omega^{\mathrm{F}}\times(0,T), \tag{1}$$

based on the mesh interface displacement $\mathbf{d}_{\Gamma}^{\mathrm{G}}$, that will later be related to the structure interface displacement $\mathbf{d}_{\Gamma}^{\mathrm{S}}$. This mapping (1) is arbitrary and defines the domain velocity $\mathbf{u}^{\mathrm{G}}$ by

$$\mathbf{u}^{\mathrm{G}} = \frac{\partial\boldsymbol{\varphi}}{\partial t} \quad \text{in} \quad \Omega^{\mathrm{F}}\times(0,T), \tag{2}$$

which has to match the fluid velocity $\mathbf{u}_{\Gamma}^{\mathrm{F}}$ at the interface Γ, i.e.

$$\mathbf{u}_{\Gamma}^{\mathrm{F}} = \mathbf{u}_{\Gamma}^{\mathrm{G}} \quad \text{in} \quad \Gamma\times(0,T). \tag{3}$$

Equation (2) allows for the definition of the ALE convective velocity $\mathbf{c} = \mathbf{u}^{\mathrm{F}} - \mathbf{u}^{\mathrm{G}}$, representing the fluid velocity relative to the arbitrarily moving fluid domain. The Navier-Stokes equations of the fluid field hence read

$$\frac{\partial\mathbf{u}^{\mathrm{F}}}{\partial t} + \mathbf{c}\cdot\boldsymbol{\nabla}\mathbf{u}^{\mathrm{F}} - 2\nu\boldsymbol{\nabla}\cdot\boldsymbol{\varepsilon}(\mathbf{u}^{\mathrm{F}}) + \nabla p^{\mathrm{F}} = \mathbf{b}^{\mathrm{F}}, \tag{4}$$

$$\boldsymbol{\nabla}\cdot\mathbf{u}^{\mathrm{F}} = 0, \tag{5}$$

both valid in $\Omega^{\mathrm{F}}\times(0,T)$, where fluid velocity $\mathbf{u}^{\mathrm{F}}$ and kinematic fluid pressure p^{F} are unknown. In the momentum equation (4), $\mathbf{b}^{\mathrm{F}}$ denotes a body force, $\boldsymbol{\varepsilon}(\mathbf{u}^{\mathrm{F}}) = \frac{1}{2}\left(\boldsymbol{\nabla}\mathbf{u}^{\mathrm{F}} + (\boldsymbol{\nabla}\mathbf{u}^{\mathrm{F}})^{\mathrm{T}}\right)$ the strain rate tensor of the Newtonian fluid and ν its kinematic viscosity. Equation (5) states the fluid's

incompressibility deduced from the conservation of mass and a constant density ρ^{F}. The fluid system is completed by the usual Dirichlet and Neumann boundary conditions and an initial divergence-free velocity field $\mathbf{u}_0^{\mathrm{F}}$.

The weak form of the incompressible Navier-Stokes equations (4) and (5) is obtained by testing these equations with test functions $\delta\mathbf{u}^{\mathrm{F}}$ for velocity and δp^{F} for pressure and subsequent integration by parts

$$\begin{aligned} 0 = &\left(\delta\mathbf{u}^{\mathrm{F}}, \frac{\partial\mathbf{u}^{\mathrm{F}}}{\partial t}\right)_{\Omega^{\mathrm{F}}} + \left(\delta\mathbf{u}^{\mathrm{F}}, \mathbf{c}\cdot\nabla\mathbf{u}^{\mathrm{F}}\right)_{\Omega^{\mathrm{F}}} + \left(\nabla\delta\mathbf{u}^{\mathrm{F}}, 2\nu\boldsymbol{\varepsilon}(\mathbf{u}^{\mathrm{F}})\right)_{\Omega^{\mathrm{F}}} - \left(\nabla\cdot\delta\mathbf{u}^{\mathrm{F}}, p^{\mathrm{F}}\right)_{\Omega^{\mathrm{F}}} \\ &- \left(\delta\mathbf{u}^{\mathrm{F}}, \mathbf{b}^{\mathrm{F}}\right)_{\Omega^{\mathrm{F}}} - \left(\delta p^{\mathrm{F}}, \nabla\cdot\mathbf{u}^{\mathrm{F}}\right)_{\Omega^{\mathrm{F}}} + \left(\delta\mathbf{u}^{\mathrm{F}}, \bar{\mathbf{h}}^{\mathrm{F}}\right)_{\Gamma_{\mathrm{N}}^{\mathrm{F}}} + \delta W_{\Gamma}^{\mathrm{F}}, \end{aligned} \tag{6}$$

where $\Gamma_{\mathrm{N}}^{\mathrm{F}}$ denotes the Neumann boundary and $\delta W_{\Gamma}^{\mathrm{F}}$ denotes a contribution of the FSI interface that will be deduced in section 2.3.

2.2 Structure

In this work we assume a structure field governed by the nonlinear elastodynamics equation

$$\rho^{\mathrm{S}}\frac{\mathrm{d}^2\mathbf{d}^{\mathrm{S}}}{\mathrm{d}t^2} = \nabla\cdot(\mathbf{FS}) + \rho^{\mathrm{S}}\mathbf{b}^{\mathrm{S}} \quad \text{in} \quad \Omega^{\mathrm{S}}\times(0,T), \tag{7}$$

which states an equilibrium between the forces of inertia, internal forces and an external body force $\mathbf{b}^{\mathrm{S}}$ in the undeformed structural configuration Ω^{S}. Given the structural density ρ^{S} defined per unit undeformed volume, equation (7) has to be solved for the unknown structural displacements $\mathbf{d}^{\mathrm{S}}$. The internal forces are expressed in terms of the second Piola-Kirchhoff stress tensor $\mathbf{S}$ and the deformation gradient $\mathbf{F}$.

Different constitutive relations can be employed in this context, but for the sake of simplicity a hyperelastic material behavior with strain energy function Ψ is considered in the remainder of this paper. The second Piola-Kirchhoff stress tensor $\mathbf{S}$ is thus defined as

$$\mathbf{S} = 2\frac{\partial\Psi}{\partial\mathbf{C}}, \tag{8}$$

where the right Cauchy-Green tensor $\mathbf{C} = \mathbf{F}^{\mathrm{T}}\mathbf{F}$ has been introduced. Dirichlet and Neumann boundary conditions as well as the usual initial boundary conditions, given initial displacements and velocities $\mathbf{d}_0^{\mathrm{S}}$ and $\dot{\mathbf{d}}_0^{\mathrm{S}}$, respectively, have to be additionally satisfied.

Testing (7) with the virtual displacements $\delta\mathbf{d}^{\mathrm{S}}$ and integration by parts yield the weak form

$$0 = \left(\delta\mathbf{d}^{\mathrm{S}}, \rho^{\mathrm{S}}\frac{\mathrm{d}^2\mathbf{d}^{\mathrm{S}}}{\mathrm{d}t^2}\right)_{\Omega^{\mathrm{S}}} + \left(\nabla\delta\mathbf{d}^{\mathrm{S}}, \mathbf{FS}\right)_{\Omega^{\mathrm{S}}} - \left(\delta\mathbf{d}^{\mathrm{S}}, \rho^{\mathrm{S}}\mathbf{b}^{\mathrm{S}}\right)_{\Omega^{\mathrm{S}}} - \left(\delta\mathbf{d}^{\mathrm{S}}, \bar{\mathbf{h}}^{\mathrm{S}}\right)_{\Gamma_{\mathrm{N}}^{\mathrm{S}}} + \delta W_{\Gamma}^{\mathrm{S}}, \tag{9}$$

where $\Gamma_{\mathrm{N}}^{\mathrm{S}}$ denotes the Neumann boundary. The influence of the interface on the structure field is accounted for by $\delta W_{\Gamma}^{\mathrm{S}}$, which will be discussed in the following subsection.

2.3 Fluid-Structure Interface

Coupling of the different fields is realized by enforcing kinematic and dynamic constraints at the fluid-structure interface Γ. Usually, the no-slip boundary condition

$$\frac{\partial\mathbf{d}_{\Gamma}^{\mathrm{S}}}{\partial t} = \mathbf{u}_{\Gamma}^{\mathrm{F}} \quad \text{in} \quad \Gamma\times(0,T) \tag{10}$$

is applied, which prohibits both a mass flow across and a relative tangential movement of fluid and structure at the fluid-structure interface. In combination with (3) this condition (10) is equivalent to

$$\mathbf{d}_\Gamma^{\mathrm{S}} = \mathbf{d}_\Gamma^{\mathrm{G}} \quad \text{in} \quad \Gamma \times (0,T), \tag{11}$$

stating that structural deformation and fluid movement (represented by the ALE based fluid domain deformation $\mathbf{d}_\Gamma^{\mathrm{G}}$) must match on Γ. In addition, equilibrium of forces requires the surface tractions of fluid and structure to be equal, yielding

$$\mathbf{h}_\Gamma^{\mathrm{S}} = -\mathbf{h}_\Gamma^{\mathrm{F}} \quad \text{in} \quad \Gamma \times (0,T). \tag{12}$$

In preparation of the mortar finite element discretization to follow, the method of weighted residuals is applied to the interface conditions. By introducing the Lagrange multiplier field $\boldsymbol{\lambda}$ and corresponding test functions $\delta\boldsymbol{\lambda}$ on the fluid-structure interface Γ, we obtain the weak form

$$\left(\delta\boldsymbol{\lambda}, \mathbf{d}_\Gamma^{\mathrm{S}} - \mathbf{d}_\Gamma^{\mathrm{G}}\right)_\Gamma = 0. \tag{13}$$

This adds an integral version of the continuity constraint (11) to the general problem definition. Furthermore, the unknown surface tractions introduced in (12) have to be imposed in a weak sense on the respective physical field, yielding the missing coupling terms in fluid weak form (6) and structure weak form (9)

$$\delta W_\Gamma^{\mathrm{F}} = \left(\mathbf{h}_\Gamma^{\mathrm{F}}, \delta\mathbf{u}_\Gamma^{\mathrm{F}}\right)_\Gamma, \tag{14}$$

$$\delta W_\Gamma^{\mathrm{S}} = \left(\mathbf{h}_\Gamma^{\mathrm{S}}, \delta\mathbf{d}_\Gamma^{\mathrm{S}}\right)_\Gamma. \tag{15}$$

Identifying the Lagrange multiplier field $\boldsymbol{\lambda}$ with the unknown surface traction $\mathbf{h}_\Gamma^{\mathrm{S}} = -\mathbf{h}_\Gamma^{\mathrm{F}}$, these coupling terms can be expressed as

$$\delta W_\Gamma^{\mathrm{F}} = -\left(\boldsymbol{\lambda}, \delta\mathbf{u}_\Gamma^{\mathrm{F}}\right)_\Gamma, \tag{16}$$

$$\delta W_\Gamma^{\mathrm{S}} = \left(\boldsymbol{\lambda}, \delta\mathbf{d}_\Gamma^{\mathrm{S}}\right)_\Gamma. \tag{17}$$

Thus, fluid-structure coupling is established in a weak sense, which formally leads to a four field FSI system.

3 DISCRETIZATION AND SOLUTION ALGORITHM

3.1 The monolithic FSI system

To derive the monolithic FSI system of equations, the governing equations stated above are discretized in space and time and the resulting non-linear equations are linearized consistently in order to apply a Newton-Raphson algorithm. Note that the presented algorithm is not limited to a particular choice of these discretizations. In general, we use finite element discretizations for fluid, ALE and structure fields and implicit time integration schemes.

The final linear system of equation for timestep $n+1$ and iteration step i then emerges as

$$\begin{bmatrix} \mathbf{S}_{\mathrm{II}} & \mathbf{S}_{\mathrm{I\Gamma}} & & & & \\ \mathbf{S}_{\mathrm{\Gamma I}} & \mathbf{S}_{\mathrm{\Gamma\Gamma}} & & & & \mathbf{C}_{\mathrm{S}}^{\mathrm{T}} \\ & & \mathbf{F}_{\mathrm{II}} & \mathbf{F}_{\mathrm{I\Gamma}} + \frac{\Delta t}{2}\mathbf{F}_{\mathrm{I\Gamma}}^{\mathrm{G}} & \mathbf{F}_{\mathrm{II}}^{\mathrm{G}} & \\ & & \mathbf{F}_{\mathrm{\Gamma I}} & \mathbf{F}_{\mathrm{\Gamma\Gamma}} + \frac{\Delta t}{2}\mathbf{F}_{\mathrm{\Gamma\Gamma}}^{\mathrm{G}} & \mathbf{F}_{\mathrm{\Gamma I}}^{\mathrm{G}} & -\mathbf{C}_{\mathrm{F}}^{\mathrm{T}} \\ & & \mathbf{0} & \frac{\Delta t}{2}\mathbf{A}_{\mathrm{I\Gamma}} & \mathbf{A}_{\mathrm{II}} & \\ & \mathbf{C}_{\mathrm{S}} & & -\frac{\Delta t}{2}\mathbf{C}_{\mathrm{F}} & & \end{bmatrix} \begin{bmatrix} \Delta\mathbf{d}_{\mathrm{I},i}^{\mathrm{S},n+1} \\ \Delta\mathbf{d}_{\mathrm{\Gamma},i}^{\mathrm{S},n+1} \\ \Delta\mathbf{u}_{\mathrm{I},i}^{\mathrm{F},n+1} \\ \Delta\mathbf{u}_{\mathrm{\Gamma},i}^{\mathrm{F},n+1} \\ \Delta\mathbf{d}_{\mathrm{I},i}^{\mathrm{G},n+1} \\ \boldsymbol{\lambda}_i^{n+1} \end{bmatrix} =$$

$$- \begin{bmatrix} \mathbf{f}_{\mathrm{I},i}^{\mathrm{S},n+1} \\ \mathbf{f}_{\mathrm{\Gamma},i}^{\mathrm{S},n+1} \\ \mathbf{f}_{\mathrm{I},i}^{\mathrm{F},n+1} \\ \mathbf{f}_{\mathrm{\Gamma},i}^{\mathrm{F},n+1} \\ \mathbf{0} \\ \mathbf{0} \end{bmatrix} - \delta_{i0}\Delta t \begin{bmatrix} \mathbf{0} \\ \mathbf{0} \\ \mathbf{F}_{\mathrm{I\Gamma}}^{\mathrm{G}}\mathbf{u}_{\mathrm{\Gamma}}^{\mathrm{F},n} \\ \mathbf{F}_{\mathrm{\Gamma\Gamma}}^{\mathrm{G}}\mathbf{u}_{\mathrm{\Gamma}}^{\mathrm{F},n} \\ \mathbf{A}_{\mathrm{I\Gamma}}\mathbf{u}_{\mathrm{\Gamma}}^{\mathrm{F},n} \\ \mathbf{C}_{\mathrm{F}}\mathbf{u}_{\mathrm{\Gamma}}^{\mathrm{F},n} \end{bmatrix}, \tag{18}$$

where δ_{i0} denotes the Kronecker delta. In equation (18) the vector of unknowns and the right-hand side are split in quantities defined on the FSI interface denoted by $\cdot_{\Gamma}$ and in the interior field denoted by $\cdot_{\mathrm{I}}$. This split then propagates to the matrix block structure. The block structure of the structure stiffness matrix $\mathbf{S}$ is defined as $\mathbf{S}_{\alpha\beta} = \partial\mathbf{f}_{\alpha}^{\mathrm{S}}/\partial\mathbf{d}_{\beta}^{\mathrm{S}}$, $\alpha,\beta \in \{\mathrm{I},\Gamma\}$, where $\mathbf{f}^{\mathrm{S}}$ denotes the residual vector and $\mathbf{d}^{\mathrm{S}}$ the vector of discretized nodal displacements. To shorten the notation for the fluid part, we have merged the pressure degrees of freedom into the vector of fluid interior unknowns. Fluid entries are then defined as $\mathbf{F}_{\alpha\beta} = \partial\mathbf{f}_{\alpha}^{\mathrm{F}}/\partial\mathbf{u}_{\beta}^{\mathrm{F}}$ and shape derivatives as $\mathbf{F}_{\alpha\beta}^{\mathrm{G}} = \partial\mathbf{f}_{\alpha}^{\mathrm{F}}/\partial\mathbf{d}_{\beta}^{\mathrm{G}}, \alpha,\beta \in \{\mathrm{I},\Gamma\}$. Here, $\mathbf{f}^{\mathrm{F}}$ denotes the fluid residual, $\mathbf{u}^{\mathrm{F}}$ the vector of discretized fluid unknowns and $\mathbf{d}^{\mathrm{G}}$ the vector of fluid grid displacements. The ALE system matrix $\mathbf{A}$ is split accordingly into blocks $\mathbf{A}_{\mathrm{I\Gamma}}$ and $\mathbf{A}_{\mathrm{II}}$.

The system is completed by coupling matrices $\mathbf{C}_{\mathrm{S}}$ and $\mathbf{C}_{\mathrm{F}}$. The last row of (18) weakly imposes the continuity constraint (11) and thus represents the discrete version of (13). The contributions of the vector of discretized Lagrange multiplier values $\boldsymbol{\lambda}$, i.e. $-\mathbf{C}^{\mathrm{F}}\boldsymbol{\lambda}$ and $\mathbf{C}^{\mathrm{S}}\boldsymbol{\lambda}$, account for the additional surface tractions on the fluid and structure field, respectively, which result from the coupling at the FSI interface and correspond to (16) and (17).

3.2 Dual mortar coupling

Non-conforming finite element discretization brings about that fluid and structure surfaces at the FSI interface Γ do not match any more, as it is the case when using node-matching interface meshes. For making the following derivations more general, we define so-called *slave* and *master* sides Γ^{sl} and Γ^{ma}, introduce the displacement fields $\mathbf{d}_{\Gamma}^{\mathrm{sl}}$ and $\mathbf{d}_{\Gamma}^{\mathrm{ma}}$ and derive the dual mortar method as an abstract coupling strategy for two non-conforming meshes. The general form of slave and master displacement interpolation then reads

$$\mathbf{d}_{\Gamma}^{\mathrm{sl}} = \sum_{k=1}^{n^{\mathrm{sl}}} N_k^{\mathrm{sl}}\mathbf{d}_k^{\mathrm{sl}}, \quad \mathbf{d}_{\Gamma}^{\mathrm{ma}} = \sum_{l=1}^{n^{\mathrm{ma}}} N_l^{\mathrm{ma}}\mathbf{d}_l^{\mathrm{ma}}, \tag{19}$$

where shape functions N_k^{sl}, N_l^{ma} are obtained based on their trace space relationship with the underlying discretizations of the domains 'behind' the mortar interface (in this context fluid

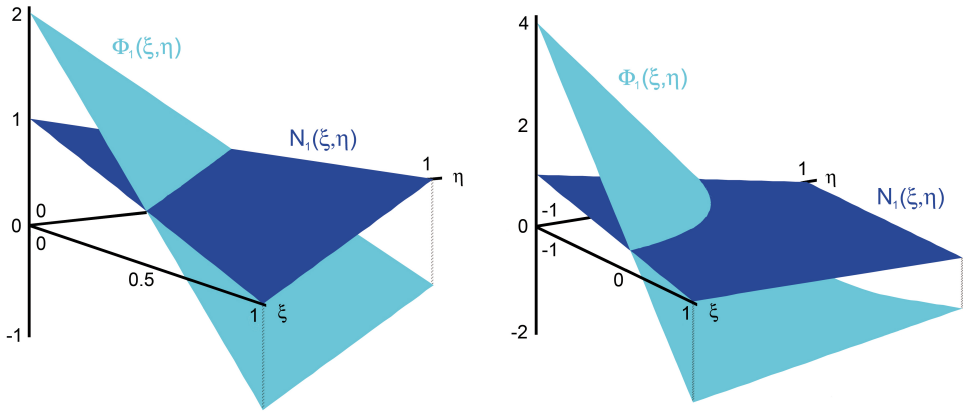

(a) 3-node triangular surface elements (b) 4-node quadrilateral surface elements

Figure 1: Exemplary shape functions $N_1(\xi,\eta)$ and dual shape functions $\Phi_1(\xi,\eta)$.

and structure domains). Nodal displacements are represented by $\mathbf{d}_k^{\mathrm{sl}}$, $\mathbf{d}_l^{\mathrm{ma}}$. The total number of slave and master nodes is given by n^{sl} and n^{ma}, respectively.

Within the *dual* mortar method considered here, the Lagrange multiplier interpolation on the slave side of the interface is based on so-called dual shape functions Φ_j as

$$\boldsymbol{\lambda} = \sum_{j=1}^{n^{\mathrm{sl}}} \Phi_j \boldsymbol{\lambda}_j \,, \tag{20}$$

with discrete nodal Lagrange multipliers $\boldsymbol{\lambda}_j$. The dual shape functions are constructed such that a biorthogonality condition, as introduced in [20, 13, 14], is satisfied, yielding

$$\int_{\Gamma^{\mathrm{sl}}} \Phi_j N_k^{\mathrm{sl}} \mathrm{d}\Gamma = \delta_{jk} \int_{\Gamma^{\mathrm{sl}}} N_k^{\mathrm{sl}} \mathrm{d}\Gamma, \tag{21}$$

where δ_{jk} is the Kronecker delta. Note that (21) demands an evaluation of shape function integrals on the actual (possibly distorted) surface element geometry in the reference configuration. Therefore, an *a priori* definition of dual shape functions is not possible in general, but these ansatz functions for Lagrange multiplier interpolation become element-specific. Fig. 1 exemplarily shows (standard) displacement shape functions and (dual) Lagrange multiplier shape functions for a 3-node triangular and for an undistorted 4-node quadrilateral surface element. For a more detailed overview and exemplary local calculations of element-specific dual shape functions for 3D mortar coupling, we refer to [11, 8].

For the sake of clarity, we temporarily ignore the weak continuity condition (13) already derived for the concrete FSI setting and instead consider the more general form

$$\left(\delta\boldsymbol{\lambda}, \mathbf{d}_\Gamma^{\mathrm{sl}} - \mathbf{d}_\Gamma^{\mathrm{ma}}\right)_\Gamma = 0 \tag{22}$$

in the following, which couples slave and master displacements of an abstract non-conforming interface. When the interpolations (19) and (20) are substituted into (22), the nodal blocks of two mortar integral matrices $\mathbf{D}$ and $\mathbf{M}$ emerge as

$$\mathbf{D}[j,k] = \mathrm{D}_{jk}\mathbf{I}_3 = \int_{\Gamma^{\mathrm{sl}}} \Phi_j N_k^{\mathrm{sl}} \mathrm{d}\Gamma \, \mathbf{I}_3 \,, \tag{23}$$

$$\mathbf{M}[j,l] = \mathrm{M}_{jl}\mathbf{I}_3 = \int_{\Gamma^{\mathrm{sl}}} \Phi_j N_l^{\mathrm{ma}} \mathrm{d}\Gamma \, \mathbf{I}_3 \,, \tag{24}$$

with the 3×3 identity matrix $\mathbf{I}_3$. Herein, $\mathbf{D}$ is a square $3n^{\mathrm{sl}} \times 3n^{\mathrm{sl}}$ matrix, whereas the definition of $\mathbf{M}$ generally yields a rectangular matrix of dimensions $3n^{\mathrm{sl}} \times 3n^{\mathrm{ma}}$. Inserting the biorthogonality relation (21) into (23) allows for the advantageous simplification of $\mathbf{D}$ to become a diagonal matrix with nodal blocks

$$\mathbf{D}[j,k] = \mathrm{D}_{jk}\mathbf{I}_3 = \delta_{jk} \int_{\Gamma^{\mathrm{sl}}} N_k^{\mathrm{sl}} \mathrm{d}\Gamma \, \mathbf{I}_3 \,. \tag{25}$$

Finally, the discrete form of the general weak continuity condition (22) reads

$$\mathbf{D}\mathbf{d}_{\Gamma}^{\mathrm{sl}} - \mathbf{M}\mathbf{d}_{\Gamma}^{\mathrm{ma}} = \mathbf{0}, \tag{26}$$

which naturally defines a discrete projection from master to slave displacements as

$$\mathbf{d}_{\Gamma}^{\mathrm{sl}} = \mathbf{D}^{-1}\mathbf{M}\mathbf{d}_{\Gamma}^{\mathrm{ma}}. \tag{27}$$

Equation (27) illustrates one major advantage of the dual mortar approach as compared with standard mortar schemes. The discrete projection operator $\mathbf{P} = \mathbf{D}^{-1}\mathbf{M}$ at a non-conforming interface can be applied locally based on the trivial inversion of the diagonal matrix $\mathbf{D}$. Thus, evaluating (27) does not require the solution of a possibly large linear system of equations. This evades the high computational cost associated with standard mortar coupling of two non-conforming grids. Note that depending on the choice of structure or fluid as slave side for the mortar approach, the discrete coupling matrices $\mathbf{C}_{\mathrm{S}}$ and $\mathbf{C}_{\mathrm{F}}$ in (18) can be identified with the mortar matrices $\mathbf{D}$ and $\mathbf{M}$.

3.3 Condensed linear system

The four-field linear system in (18) is in general very hard to solve numerically with parallel iterative linear solvers, because of the saddle point type structure of the problem. Since larger model sizes necessitate this type of solvers, the linear system is transformed into the same block-structure as the standard monolithic FSI system for conforming discretizations shown in [5]. The transformation is based on condensation of the Lagrange multipliers, which is only possible due to the dual mortar approach discussed in section 3.2.

Of course both choices for master and slave side of the mortar coupling are possible and result in viable algorithms as has been shown in great detail in [1]. For the sake of brevity, in this contribution only one possibility is discussed: we assume that the structure side of the FSI interface Γ serves as slave side for the mortar coupling. Thus the coupling matrices in (18) can be identified as $\mathbf{C}_{\mathrm{F}} = \mathbf{M}$ and $\mathbf{C}_{\mathrm{S}} = \mathbf{D}$.

The second row of (18) is solved for the Lagrange multipliers $\boldsymbol{\lambda}_i^{n+1}$, involving a trivial inversion of the diagonal matrix $\mathbf{D}$. The result can then be substituted into the fourth row of (18), so that the Lagrange multipliers are fully eliminated from the system. A further reduction can be obtained by a transformation of the last row of (18), which allows to express the structure interface displacement updates $\Delta\mathbf{d}_{\Gamma,i}^{\mathrm{S},n+1}$ in terms of fluid interface velocity updates $\Delta\mathbf{u}_{\Gamma,i}^{\mathrm{F},n+1}$.

Subsequent substitution and reordering yield the final reduced system of equations

$$\begin{bmatrix} \mathbf{S}_{\mathrm{II}} & \frac{\Delta t}{2}\mathbf{S}_{\mathrm{I\Gamma}}\mathbf{P} & & \\ \mathbf{P}^{\mathrm{T}}\mathbf{S}_{\mathrm{\Gamma I}} & \frac{\Delta t}{2}\mathbf{P}^{\mathrm{T}}\mathbf{S}_{\mathrm{\Gamma I}}\mathbf{P}+\mathbf{F}_{\mathrm{\Gamma\Gamma}}+\frac{\Delta t}{2}\mathbf{F}^{\mathrm{G}}_{\mathrm{\Gamma\Gamma}} & \mathbf{F}_{\mathrm{\Gamma I}} & \mathbf{F}^{\mathrm{G}}_{\mathrm{\Gamma I}} \\ & \mathbf{F}_{\mathrm{I\Gamma}}+\frac{\Delta t}{2}\mathbf{F}^{\mathrm{G}}_{\mathrm{I\Gamma}} & \mathbf{F}_{\mathrm{II}} & \mathbf{F}^{\mathrm{G}}_{\mathrm{II}} \\ & \frac{\Delta t}{2}\mathbf{A}_{\mathrm{I\Gamma}} & \mathbf{0} & \mathbf{A}_{\mathrm{II}} \end{bmatrix} \begin{bmatrix} \Delta\mathbf{d}^{\mathrm{S},n+1}_{\mathrm{I},i} \\ \Delta\mathbf{u}^{\mathrm{F},n+1}_{\Gamma,i} \\ \Delta\mathbf{u}^{\mathrm{F},n+1}_{\mathrm{I},i} \\ \Delta\mathbf{d}^{\mathrm{G},n+1}_{\mathrm{I},i} \end{bmatrix} =$$
$$\begin{bmatrix} \mathbf{f}^{\mathrm{S},n+1}_{\mathrm{I},i} \\ \mathbf{f}^{\mathrm{F},n+1}_{\Gamma,i}+\mathbf{P}^{\mathrm{T}}\mathbf{f}^{\mathrm{S},n+1}_{\Gamma,i} \\ \mathbf{f}^{\mathrm{F},n+1}_{\mathrm{I},i} \\ \mathbf{0} \end{bmatrix} + \delta_{i0}\,\Delta t \begin{bmatrix} \mathbf{S}_{\mathrm{I\Gamma}}\mathbf{P}\,\mathbf{u}^{\mathrm{F},n}_{\Gamma} \\ \left(\mathbf{P}^{\mathrm{T}}\mathbf{S}_{\mathrm{\Gamma\Gamma}}\mathbf{P}+\mathbf{F}^{\mathrm{G}}_{\mathrm{\Gamma\Gamma}}\right)\mathbf{u}^{\mathrm{F},n}_{\Gamma} \\ \mathbf{F}^{\mathrm{G}}_{\mathrm{I\Gamma}}\mathbf{u}^{\mathrm{F},n}_{\Gamma} \\ \mathbf{A}_{\mathrm{I\Gamma}}\mathbf{u}^{\mathrm{F},n}_{\Gamma} \end{bmatrix}. \tag{28}$$

4 EXAMPLE

To demonstrate the efficiency of the proposed method, different discretizations of the same fluid filled circular pipe with traveling pressure wave are considered. The example is motivated by [5, 21]. The tube is 0.1 m long, has an inner radius of 0.01 m and an outer radius of 0.011 m. The structure is described with a Neo-Hookean material law with Young's modulus $E = 10^5$ Pa, Poisson's ratio $\nu = 0.3$ and a density of $\rho^{\mathrm{S}} = 1{,}200\,\mathrm{kg/m^3}$. The Newtonian fluid inside the tube has a dynamic viscosity of $\mu = 0.003\,\mathrm{Pa\,s}$ and a density of $\rho^{\mathrm{F}} = 1{,}000\,\mathrm{kg/m^3}$. The inflow surface is loaded with a surface traction of $1{,}000\,\mathrm{Pa}$ for $0.003\,\mathrm{s}$. For the computation a timestep size of $\Delta t = 1.0 \times 10^{-4}\,\mathrm{s}$ is used and 250 timesteps are performed. The fluid is discretized with stabilized hexahedral finite elements, the structure with hexahedral solid shell elements proposed in [22].

We concentrate on four fluid discretizations denoted by *A*, *B*, *C* and *D* with different mesh sizes, which range from 2,080 to 130,560 elements. For all fluid mesh sizes corresponding conforming and non-conforming structure discretizations are considered. In the non-conforming versions the structure mesh is rotated such that the meshes overlap in circumferential direction by approximately a third of an element length, see Fig. 2(a). Furthermore, it contains two elements less than the fluid discretization across the length of the tube. The coarsest non-conforming model can be seen in Fig. 2.

Computations are performed in parallel on up to 12 processors. In order to study efficiency and scalability of the proposed approach, we distinguish not only between conforming and non-conforming (NC), but consider two solution methods for the conforming case: with mortar

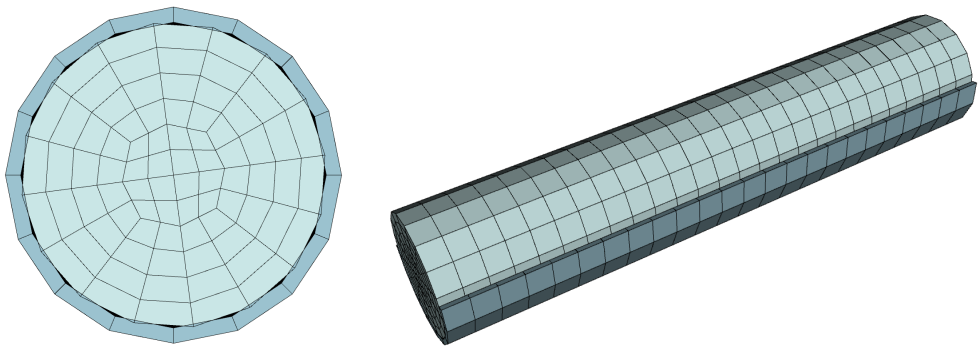

(a) front view (b) side view

Figure 2: Coarse, non-conforming mesh *A* for pressure wave example.

Table 1: Characteristics for the numerical solver averaged over timestep and number of processors used.

Mesh		n_{dof}	n_{pr}	Newton	GMRES	time
A	(C)	19,413	4	2.97	29.2	4.44
A	(CM)	19,413	4	2.97	29.2	4.56
A	(NC)	19,221	4	2.97	36.1	6.09
B	(C)	140,291	8	2.98	30.0	22.99
B	(CM)	140,291	8	2.98	30.0	23.59
B	(NC)	139,715	8	2.98	32.8	27.1
C	(C)	377,857	12	2.97	30.9	41.09
C	(CM)	377,857	12	2.97	30.9	41.43
C	(NC)	376,705	12	2.97	37.1	50.68
D	(C)	1,045,553	12	2.78	33.9	99.44
D	(CM)	1,045,553	12	2.78	33.9	101.12
D	(NC)	1,043,663	12	2.78	42.7	121.68

coupling (CM) and with the standard approach (C) presented in [5]. In all cases the AMG(BGS) preconditioner introduced in [5] is employed to solve the linear system (28). The numerical behavior is assessed by the average number of Newton iterations, the average number of GMRES iterations and the average computation time per timestep. These quantities and the total number n_{dof} of degrees of freedom are listed in Tab. 1.

As could be expected the number of Newton iterations and linear iterations of the GMRES algorithm for the two conforming meshes coincide. The mortar approach and the corresponding explicit matrix-matrix products, which are needed to eliminate the discrete Lagrange multipliers and to set up the condensed system matrices, affect the numerical costs only very slightly. The average time spent for a timestep increases by less than 2% in all cases considered, which indicates the numerical efficiency of the proposed approach. Having to deal with non-conforming meshes (rows marked with 'NC' in Tab. 1) leads to an increase in computation time of approximately 25% for this example. This is completely due to linear systems of equations that are apparently harder to solve, which becomes obvious by comparing the average number of GMRES steps and Newton steps. The relative increase of iteration steps needed in the GMRES corresponds exactly to the relative increase in computation time, whereas the number of Newton iterations is unchanged. While this increase can not be neglected, it is however important to point out that the preconditioners have not been optimized for the non-conforming case but are simply carried over from the conforming case. The computational cost associated with the evaluation of dual mortar coupling itself is virtually zero. This is above all due to the fact that the mortar integrals (i.e. matrices $\mathbf{D}$ and $\mathbf{M}$) only need to be evaluated once during problem initialization and remain unchanged during all FSI timesteps afterwards.

5 CONCLUSION

A novel mortar-based approach to efficiently simulate fluid-structure interaction phenomena allowing for independent discretization of fluid and structure domains has been presented. Owing to its generality, the proposed FSI framework does not introduce any restriction on the particular choice of finite element formulations neither for fluid, ALE nor structure. Implicit time integration is employed for all three physical fields. Consistent linearization within a Newton-Raphson scheme provides the fundamental building blocks of the monolithic system.

In contrast to available approaches in literature, the proposed formulation is based on a dual

mortar method and handles the additional complexity of non-matching interface meshes at negligible computational cost. The complete four-field monolithic system initially has a saddle point type structure, but is then transformed into a three-field system by condensation of the Lagrange multiplier degrees of freedom. The transformation requires the inversion of one of the coupling matrices, which is trivial due to its diagonal shape. This diagonality is a key feature of the dual mortar approach as opposed to standard mortar coupling schemes. Because of the transformation the application of state-of-the-art iterative solution methods to the resulting system matrices is straightforward.

In particular, block-specific preconditioners tailored for conforming monolithic FSI show excellent performance also in the non-conforming case, which is demonstrated with the well-known pressure wave example. It also shows that computational cost associated with the evaluation of dual mortar coupling itself and with the additional matrix-matrix multiplication necessary in some sub-blocks of the monolithic system is very low.

REFERENCES

[1] T. Klöppel, A. Popp, U. Küttler, W.A. Wall, Fluid-structure interaction for non-conforming interfaces based on a dual mortar formulation. *Computer Methods in Applied Mechanics and Engineering*, submitted, 2010.

[2] M. Heil, An efficient solver for the fully coupled solution of large-displacement fluid–structure interaction problems. *Computer Methods in Applied Mechanics and Engineering*, **193**, 1–23, 2004.

[3] U. Küttler, M. Gee, Ch. Förster, A. Comerford, W.A. Wall, Coupling strategies for biomedical fluid-structure interaction problems. *International Journal for Numerical Methods in Biomedical Engineering*, **26**, 305–321, 2010.

[4] T. Klöppel, W.A. Wall, A novel two-layer, coupled finite element approach for the nonlinear elastic and viscoelastic behavior of human erythrocytes. *Biomech. Model. Mechan.*, DOI: 10.1007/s10237-010-0246-2, 2010.

[5] M. W. Gee, U. Küttler, W. A. Wall, Truly monolithic algebraic multigrid for fluid-structure interaction. *Int. J. Numer. Meth. Engng.*, **85**(8), 987–1016, 2011.

[6] C. Bernardi, Y. Maday, A.T. Patera, A new nonconforming approach to domain decomposition: the mortar element method. H. Brezis, J.L. Lions eds. *Nonlinear partial differential equations and their applications*, Pitman/Wiley: London/New York, 1994.

[7] A. Popp, M.W. Gee, W.A. Wall, A finite deformation mortar contact formulation using a primal-dual active set strategy. *International Journal for Numerical Methods in Engineering*, **79**, 1354–1391, 2009.

[8] A. Popp, M. Gitterle, M.W. Gee, W.A. Wall, A dual mortar approach for 3D finite deformation contact with consistent linearization. *International Journal for Numerical Methods in Engineering*, **83**, 1428–1465, 2010.

[9] M.A. Puso, T.A. Laursen, A mortar segment-to-segment contact method for large deformation solid mechanics. *Computer Methods in Applied Mechanics and Engineering*, **193**, 601–629, 2004.

[10] M.A. Puso, T.A. Laursen, A mortar segment-to-segment frictional contact method for large deformations. *Computer Methods in Applied Mechanics and Engineering*, **193**, 4891–4913, 2004.

[11] B. Flemisch, B.I. Wohlmuth, Stable lagrange multipliers for quadrilateral meshes of curved interfaces in 3D. *Computer Methods in Applied Mechanics and Engineering*, **196**, 1589–1602, 2007.

[12] M.A. Puso, A 3D mortar method for solid mechanics. *International Journal for Numerical Methods in Engineering*, **59**, 315–336, 2004.

[13] B.I. Wohlmuth, A mortar finite element method using dual spaces for the Lagrange multiplier. *SIAM Journal on Numerical Analysis*, **38**, 989–1012, 2000.

[14] B.I. Wohlmuth, *Discretization methods and iterative solvers based on domain decomposition*. Springer-Verlag Berlin Heidelberg, 2001.

[15] A. de Boer, A.H. van Zuijlen, H. Bijl, Review of coupling methods for non-matching meshes. *Computer Methods in Applied Mechanics and Engineering*, **196**, 1515–1525, January 2007.

[16] W. Dettmer, D. Peric, A computational framework for fluid-structure interaction: Finite element formulation and applications. *Computer Methods in Applied Mechanics and Engineering*, **195**, 5754–5779, 2006.

[17] C. Farhat, M. Lesoinne, P. Le Tallec, Load and motion transfer algorithms for fluid/structure interaction problems with non-matching discrete interfaces: Momentum and energy conservation, optimal discretization and application to aeroelasticity. *Computer Methods in Applied Mechanics and Engineering*, **157**, 95–114, 1998.

[18] H.-G. Kim, A new coupling strategy for fluid-solid interaction problems by using the interface element method. *International Journal for Numerical Methods in Engineering*, **81**, 403–428, 2010.

[19] M.R. Ross, M.A. Sprague, C.A. Felippa, K.C. Park, Treatment of acoustic fluid-structure interaction by localized lagrange multipliers and comparison to alternative interface-coupling methods. *Computer Methods in Applied Mechanics and Engineering*, **198**, 986–1005, 2009.

[20] S. Hüeber, B.I. Wohlmuth, A primal-dual active set strategy for non-linear multibody contact problems. *Computer Methods in Applied Mechanics and Engineering*, **194**, 3147–3166, 2005.

[21] J.F. Gerbeau, M. Vidrascu, A quasi-Newton algorithm based on a reduced model for fluid-structure interaction problems in blood flow. *Mathematical Modelling and Numerical Analysis*, **37**(4), 631–647, 2003.

[22] L. Vu-Quoc, X.G. Tan, Optimal solid shells for non-linear analyses of multilayer composites. i. statics. *Computer Methods in Applied Mechanics and Engineering*, **192**, 975–1016, 2003.